

IDETC2019-98109

DESIGN, MODELING, AND OPTIMIZATION OF A HOPPING ROBOT PLATFORM

Jacob W. Knaup

Student

Ira A. Fulton Schools of Engineering
Arizona State University
Tempe, Arizona
Email: jknaup@asu.edu

Daniel M. Aukes

Assistant Professor

Ira A. Fulton Schools of Engineering
Arizona State University
Tempe, Arizona
Email: danaukes@asu.edu

ABSTRACT

Laminate devices have the potential to lower the cost and complexity of robots. Taking advantage of laminate materials' flexibility, a high-performance jumping platform has been developed with the goal of optimizing jump ground clearance. Four simulations are compared in order to understand which dynamic model elements (leg flexibility, motor dynamics, contact, joint damping, etc.) must be included to accurately model jumping performance. The resulting simulations have been validated with experimental data gathered from a small set of physical leg prototypes spanning design considerations such as gear ratio and leg length, and one in particular was selected for the fidelity of performance trends against experimental results. This simulation has subsequently been used to predict the performance of new leg designs outside the initial design set. The design predicted to achieve the highest jump ground clearance was then built and tested as a demonstration of the usefulness of this simulation.

harmful situations such as mine detection or search and rescue, cases in which there is a high risk that the robot could be irrecoverably lost or damaged [1]. The individual complexity and cost of these robots also renders them impractical for swarm applications, where complex tasks are achieved by a large pool of simpler, more cost-effective robots. Additionally, conventional walking robots' large, rigid frames make them difficult to store and transport from one location to another.

Foldable laminate robots offer a low-cost, lightweight alternative to conventional rigid robots. Laminate robots can be manufactured using affordable, readily-available materials and commercially available laser cutters [2]. However, laminate robots face challenges balancing performance, cost, durability, manufacturability, and size. Extremely small robots may achieve high levels of performance, but are difficult and expensive to manufacture. Larger robots may be easier to manufacture with widely available rapid prototyping tools, but push the limits of stiffness achievable with low-cost materials.

Researchers at Worcester Polytechnic Institute have developed a foldable hexapod robot capable of locomotion at a speed of five body-lengths per second. However, their design has a ground clearance of only 15mm rendering it unable to traverse uneven terrain [2]. One robot showing signs of promise is DASH. Developed by researchers at UC Berkeley, this foldable robot utilizes a leg design inspired by the cockroach to achieve speeds up to 1.5 m/s and can scale obstacles greater than its own height [3]. Many traditional bio-inspired robots employ jumping as an alternative to climbing for scaling large obstacles, such as [4], the

1 Introduction

Legged robots offer the potential to navigate variable terrain that conventional wheeled and tracked robots cannot. Even at small scales, a legged design offers the potential to scale larger obstacles relative to the robot's size due to the ability to perform maneuvers such as jumping, hopping, and climbing. However, with this increased mobility comes a trade-off; legged robots are typically complex, rendering them expensive and bulky. The high cost of these robots makes them less suitable for potentially

MSU Jumper [5], [6], [7], the millimeter-scale Grillo [8], the 7g jumper [9], and a flea-inspired jumper [10]. These robots, however, all rely on storing energy in a discrete spring to achieve jumping, and are thus limited in their jumping frequency by the time needed to charge the spring and cannot perform natural, continuous movements. Several larger, traditional, bio-inspired robots utilize directly-actuated legs. One example is Mowgli, which uses specialized pneumatic actuators [11] and ATRIAS, which includes inline springs directly-driven by the main actuators [12]. Several small robots which do not rely on elastic energy storage are [13] which uses custom variable gears to maximize the torque generated throughout leg extension, Salto which also uses a variable gear ratio and includes series springs [14], and Minitaur which uses high-end brushless motors to generate high torque without the need for a gear reduction [15].

Our research attempts to strike a balance between complexity and performance with a centimeter-scale robot design that uses two gear-motors in conjunction with a laminate five-bar mechanism that can be manufactured using a commercially available laser cutter and heat press. Keeping with the theme of low-cost fabrication, less-rigid materials along with hobby-grade motors are considered for the design of this robot. Because a completely rigid robot leg would increase leg mass, material cost, and design complexity, our approach is to design a system with cheaper materials that are more easily cut but carry along with them some flexibility. Our approach is to understand and leverage that flexibility for the creation of dynamic elements, such as links, dampers, and springs, within a monolithic leg design constructed using laminate processes. Therefore, a leg with flexibility built into its design, if optimized, may be considered an effective means of balancing performance and value. Likewise in selecting motors, our design process seeks to capture as much performance as possible by considering the optimal gear ratio for jumping for a low-cost, hobby-grade motor. The goal of this research is to develop an understanding of how different design variables of a laminate robot's leg affect its performance in order to capture as much performance as possible from a given design space driven by cost and manufacturability.

To that end, this paper is organized as follows. Section 2.1 presents a description of the leg design under consideration. Section 2.2 describes initial modeling required to understand how design parameters affect performance. Following this initial thought experiment, four rigorous simulations are developed in Section 2.3. Each simulation attempts to model additional factors not included in the initial modeling such as leg inertia, ground contact, motor dynamics, and joint damping. Section 3 presents three experiments (hopping, isolated motor analysis, and inverted leg pull-ups) that were used to parameterize and validate these simulations. Section 4 compares the simulations' results with the experimental results, explains sources of error, and illustrates the final, best-fitting simulation. This final simulation is used to search the design space for the optimal jumper, which is built and

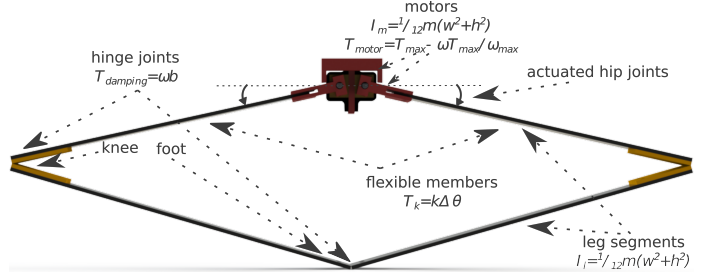


FIGURE 1: Leg design is a five-bar mechanism driven by two DC motors at the hip to allow potential actuated walking, hopping, and jumping motions in addition to vertical jumping, which is the only motion explored in this work. Non-actuated joints and leg members are made from laminate construction utilizing polyester and fiberglass respectively. The motors are connected to the laminate materials using structures 3D printed from PLA which also serve to limit the range of motion of the motors to the desired region.

tested. Section 5 summarizes the results and illustrates how the resulting simulation can be used as a tool for future efforts.

2 Description of Method

2.1 Design Process

Starting with the goal of developing a high-performance platform for legged locomotion utilizing laminate construction techniques, a platform suitable for dynamic hopping has been developed around a two degree-of-freedom leg concept shown in Figure 1. The leg is designed to allow energy from hopping to be stored in the elastic deformation of the laminate structure, utilizing laminate materials' inherent flexibility as a spring. Four segments constructed using laminate methods are connected by three joints and driven by two motors located at the hip, allowing for controllable vertical and horizontal movement in the future. The lengths of leg segments and the motor's gear ratio were both considered in our modeling and experimentation. Two design objectives were identified as well: the maximum height of our robot's center of mass and the maximum clearance of the leg during a jump.

2.2 Models

To investigate how the design variables affect the leg's performance, a simple scenario of the leg performing a single jump from a crouched position was considered. In order to gain an intuitive understanding of how the variables affect the maximum height of the foot off the ground (ground clearance), the motors' ability to apply a vertical force through the leg as the leg extends was analyzed. A highly simplified model which assumed all of the leg's mass was contained in a single point was used in this

initial thought experiment.

Because laminate structures are inherently soft, it becomes necessary to consider the flexibility of the links in order to fully capture that effect. The energy stored in the deflection of the leg's laminate structure has been modeled using a torsional spring constant to relate the restorative torque applied by the deflected leg segment to the angular deflection of the segment. This allows the torque-deflection relationship for a given structure to be determined experimentally by applying several known torques and measuring the resulting deflection.

Our model includes an energy storage and projectile phase. In the energy storage phase, the torques applied by motors at the hip joint, given by (1), are applied as a vertical force to the tip of the leg. As the leg extends and the motor velocity increases, the motor's torque decreases and the gear ratio created by the angles of the leg joints increases to apply more force for a given torque as given by (2).

$$T = T_{max} - \omega T_{max}/\omega_{max} \quad (1)$$

$$F = T \cos \theta / l - mg \quad (2)$$

Where T represents the torque produced by the motor, T_{max} is the motor's maximum rated torque for a given gear ratio, ω is the motor's angular velocity, ω_{max} is the motor's rated maximum angular velocity for a given gear-head, F is the vertical force applied to the mass, θ is the leg's angular position, l is the leg length, and m is the mass of the jumper.

In order to account for the flexibility of the leg members, the top two members are split in half - that is, each body is represented as two bodies - and connected by a linear rotational spring that pulls the bodies towards a coplanar position.

Solving the system for velocity and the angle of the hip joints allows the force to be calculated incrementally as the motor angular velocity and leg orientation changes as the leg extends. The final velocity resulting from this once the leg is fully extended is then used in an energy-based ballistic model to determine the maximum height reached by the point-mass.

The results of running this model across a variety of gear ratios and leg length combinations are shown in Figure 2. As expected, there is a trade-off between the two design variables; various combinations achieved local jump height maxima between design families. Additionally, the results showed that there is an unequal trade-off between link length and gear ratio, indicating that increasing one does not correspond linearly with increasing the other. These initial results indicate that the problem is complex and worth exploring in-depth with a multi-body simulation that more accurately represents the robot's dynamics.

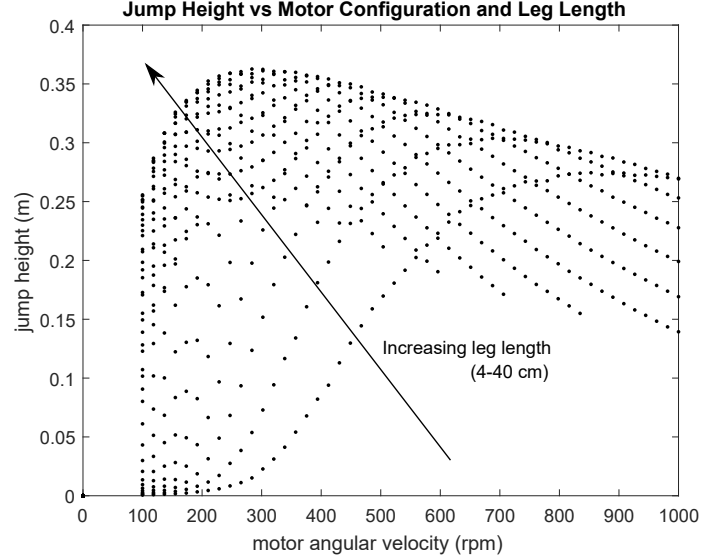


FIGURE 2: Results from initial investigation into jumping performance revealed the leg length and motor gearbox to be important design variables with nonlinear and sensitive effects on a leg's performance. Both plots show the same data set, with the left plotting the gear ratio on the x-axis and the right plotting the leg length on the x-axis. Trends seen within each plot are due to the other, complementary design variable. These initial results motivated more thorough modeling of the leg with the multi-body simulations described below.

2.3 Simulation

Four multi-body simulations were created in order to determine which elements of the robot had a significant effect on the leg's jumping performance and thus needed to be modeled in the simulation. Each simulation included separate rigid bodies with mass and inertia specified for each leg link and a body with mass and inertia to represent the two motors connected to the main body of the robot. An additional spring-loaded joint bisecting two of the segments simulates the flexibility of the leg system. The masses of each body and the spring constants for links and joints were measured for each material used. Unique additional modeling considerations were then added to each of the simulations; differences between simulations are summarized in Table 1. Each simulation was run for legs with the same set of design parameters, and each jump was started from the same crouched position. Results were then compared against experimental jumping measurements obtained for prototypes with the same leg length and gear ratio combinations in order to verify the accuracy of each simulation.

2.3.1 Simulation A The first of these simulations (A) was created in Python using a purpose-built dynamics toolkit

TABLE 1: Simulations Comparison

Simulator	Motor	Contact	Joint
	Model	Model	Damper
A	Pynamics	Linear	Spring-damper
B	Pynamics	Complex	Spring-damper
C	Unity	Linear	Proprietary PhysX
D	Unity	Linear	Proprietary PhysX Determined from data

based on Kane’s method called (Pynamics). This simulation uses the same linear motor model described in the thought experiment above (see Equation 1). Contact with the ground is modeled using a penalty method, consisting of a linear spring and damper which becomes active when the tip of the leg passes below the ground.

Comparing results between the initial thought experiment and Simulation A shows that the single-mass model predicts larger jump heights than the multi-body model for the same leg design. Both show similar trends of an optimal length/gear ratio combination existing in the design space. One notable difference between the models is that the multi-body model reaches its optimum at a much shorter leg length and a comparably faster motor gear ratio than the single-mass model. This is (likely) because the multi-body model includes inertia and factors in the increasing mass and decreasing stiffness of longer legs, whereas the single-mass model only considers the increased total weight resulting from a longer leg length. These added considerations favor a faster motor gear ratio and a shorter leg.

In spite of the improved accuracy, both simulations overestimated the height attained by leg designs. One hypothesized explanation for this was inefficiencies due to the electro-mechanical properties of the chosen motor. Therefore, these models were included in the following model.

2.3.2 Simulation B Simulation B uses the same Pynamics-based simulation engine as in A, but utilizes a more dynamical motor model rather than the linear torque/velocity relationship used in Simulation A. The linear model assumes that a DC electric motor produces maximum torque when stationary. In reality, however, the torque produced by such a motor is dependent on the current. Due to the inductance of the motor, the current will not immediately reach its maximum value. The time it takes for the current to ramp up, therefore, will cause the leg to accelerate slower as the motors produce less than their maximum

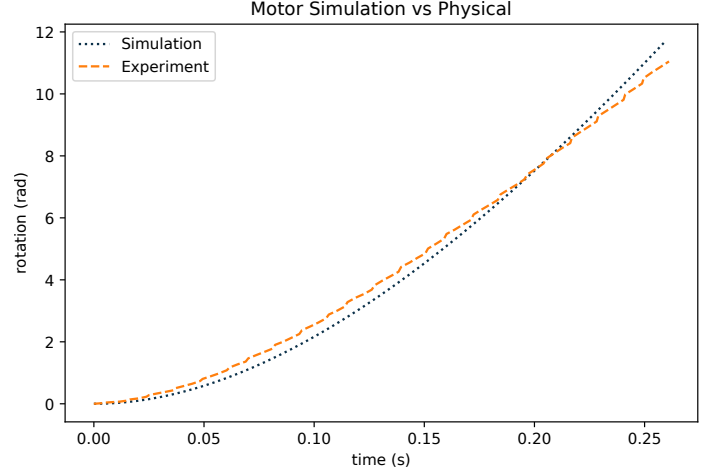


FIGURE 3: Motor model validation shows the simulation (dotted) closely matches the physical motor (dashed) when made to accelerate an unloaded shaft from rest. This model is then used in Simulation B with the leg attached to the output shaft.

torque. The current can be expressed by the following equation,

$$di/dt = (V - iR - K_v\omega)/L \quad (3)$$

where ω is the motor shaft’s angular velocity, V is the motor’s input voltage, i is the current through the motor, R is the motor’s internal resistance, K_v is the motor’s velocity constant, and L is the internal inductance of the motor.

The acceleration of the motor is dependent not only on the current, but is also affected by friction and viscous damping in the gearbox, as well as the inertia of the motor, gears, and encoder. The angular acceleration is given by (4). Both a velocity-based damping term and a sliding friction term were included as both of these factors were found to be present during the experimentation described in Section 3.0.2.

$$\alpha = (K_t i - b\omega - f_0)/I_{motor} \quad (4)$$

Where α is the motor shaft’s angular acceleration, K_t is the motor’s back-EMF constant, i is the current through the motor, b is the viscous damping constant, ω is the motor shaft’s angular velocity, f_0 is the sliding friction torque, and I_{motor} is the inertia of the motor shaft and gearbox.

The motor model’s fidelity was then compared against an unloaded physical motor as shown in Figure 3. Even with the motor inertia selected to match the measured motor’s, the model still has a shallower curvature than the physical motor.

We kept the motor model parametric during our simulation so that the effect of different motor variables could be analyzed in

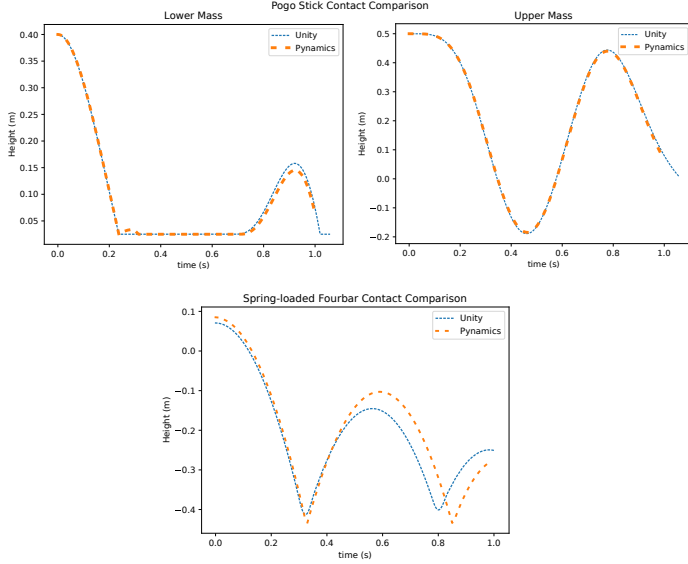


FIGURE 4: Comparison of Unity (dotted) and Pynamics (dashed) contact models shows extent of divergence. For a simple pogo stick consisting of a spring connecting two masses (top two plots), the divergence is minimal. Pynamics predicts an additional bounce upon initial contact with the ground and does not rebound as high as Unity, but the upper mass in the pogo stick is consistent between the two models. The differences become more apparent, however, with a more complex system. When a four-bar mechanism with spring-loaded joints (a simplified representation of the leg) is dropped (bottom plot) its initial contact with the ground and rebound varies considerably between the two models.

order to better understand the critical role motor selection plays in jumping performance. For example, this method revealed the importance of the motor's inductance and internal resistance in decreasing the rate at which the torque of the motor can build up from rest and highlighted the effect of changing the motor's gear-head on system acceleration.

2.3.3 Simulation C The third simulation (C) was created using the Unity game engine as a way to validate our Pynamics physics engine and compare results based on how two engines compute difficult aspects such as contact and friction. The model used in Simulation A was thus recreated in the Unity environment so that the two physics engines could be directly compared. The primary differences between the Unity and Pynamics simulators is that Unity features the PhysX real-time physics solver, useful for faster simulation, but employs an iterative optimization-based contact model that is not publicly disclosed. Pynamics permits one to explicitly or implicitly define joint constraints; the method for solving joint constraints in Unity

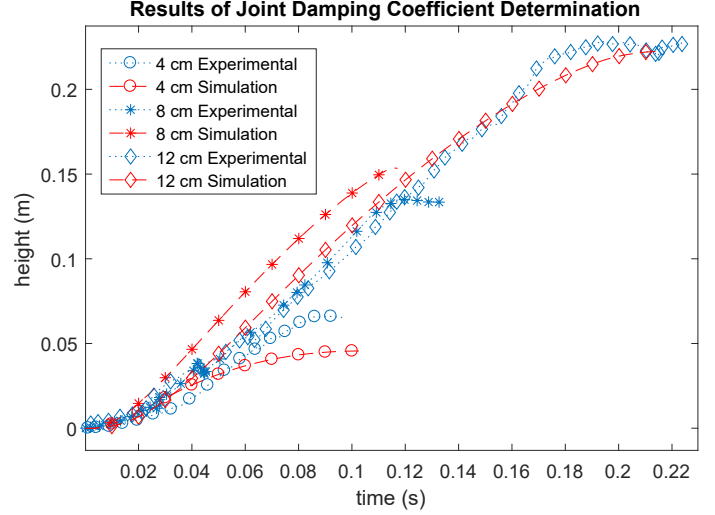


FIGURE 5: Joint damping coefficient was determined by fitting simulated pull-ups (dashed) to experimental pull-ups (dotted) with three different leg lengths (circles, stars, and diamonds). Pull-ups were used instead of jumps because they eliminated contact, slippage, tilting, and wires which were all known sources of error in jumping.

is also unknown.

To ascertain the differences between contact models for these two environments, a simple comparison was created in which a pogo stick (two masses connected by a spring) and a passive, spring-loaded four bar were dropped onto the ground and allowed to bounce. The results of this comparison are shown in Figure 4. The motion for the upper mass in the pogo stick is very similar across both simulations, but the lower mass diverges as it makes contact with and leaves the ground. The differences are even more apparent for a more complex system—the spring-loaded four bar. The system loses more energy on each bounce in Unity than in Pynamics which would suggest that Simulation C should predict lower jump heights than Simulation A. Further loss of energy is modeled in Simulation D by introducing damping.

2.3.4 Simulation D The last simulation (D) adds viscous damping to all of the joints in the laminate mechanism created in Unity. Unlike the spring constants, masses, and inertias, which could be measured directly, the damping constant was determined using a data-driven approach. A simplified version of the situation was created by inverting the leg as described in Experiment C, which eliminated some of the known sources of error in jumping. The simulated trajectories from designs using three different leg lengths were fitted to the experimental trajectories of the same designs by tuning the joint damping constant using a genetic optimization algorithm. The results of this fitting proce-

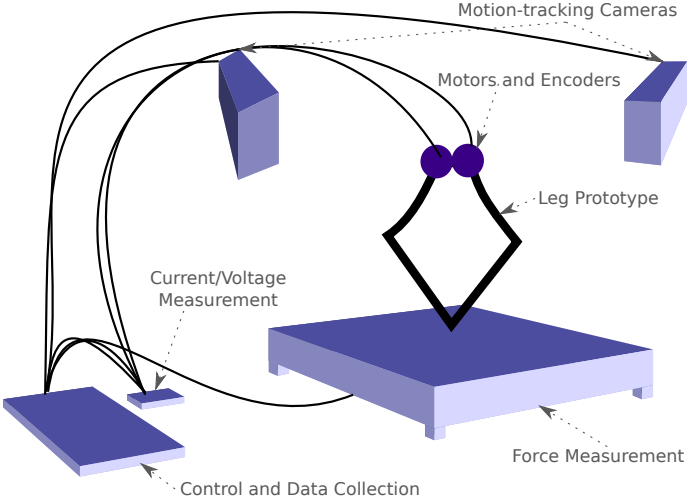


FIGURE 6: Experimental test setup of leg performing a jump from crouched position. Jump height is determined using cameras.

dure are shown in Figure 5. Once the optimal damping constant was determined, it was then used to create a new jumping representation based on Simulation C but with the addition of joint damping.

3 Experiment

3.0.1 Experiment A Experiment A was used to validate all four simulations. An experimental test setup was constructed to record the force produced by the leg, current in the motors, and the position of the leg. In each trial, the platform performs a jump starting from rest on a force plate mounted to a load cell sending real-time data to a computer. As the leg extends, a current sensor and two motor encoders record the state of the motors as shown in Figure 6. High-speed cameras track the motion of the robot body. The test is then repeated across several leg designs chosen via the simulation described above. The results of these tests are then used to verify simulation accuracy as shown in Figure 8.

3.0.2 Experiment B Experiment B was used to empirically determine the motor parameters used in Simulation B. The motor resistance was calculated by measuring the current through the motor at a given voltage while the shaft was fixed. To determine the linear relationship between the motor's voltage and rotational speed (K_v), the shaft was released and the current and angular velocity of the motor were measured at steady state for a set of given voltages. K_v could then be calculated by divid-

ing the back EMF by the angular velocity as shown in (5).

$$K_v = (V - I_{free}R) / \omega_{free} \quad (5)$$

Where K_v is the motor's back-EMF constant, V is the motor's input voltage, I_{free} is the motor's steady-state current, R is the internal resistance, and ω_{free} is the free speed.

The motor's inductance was measured directly using a L-C-R meter. The friction was determined by analyzing the current through the motor at different steady-state velocities. At constant velocity, the net torque is zero and the torque due to friction must equal the back emf torque produced by the motor as shown in (5). Without a gear head, the torque due to friction was constant once the shaft overcame static friction. This corresponds to the vertical offset in Figure 7. Once a gear-head was added, however, there was a linear relationship between the velocity of the motor's input shaft and the frictional torque as given by (6). Thus, adding a gear reduction introduces viscous friction dependent on the gear ratio.

$$T_f = K_v i_{free} = b\omega + f_0 \quad (6)$$

Where T_f is the total torque produced by friction while the motor is in motion, K_v is the motor's speed constant, i_{free} is the steady-state current in the motor, b is the viscous damping coefficient, ω is the motor's angular velocity, and f_0 is the constant torque from kinetic friction.

The inertia of the motor was found by tuning the inertia to minimize the error in the position between a simulation using all of the parameters found above and a physical motor accelerating from rest, the results of which are shown in Figure 3.

3.0.3 Experiment C Experiment C was used to determine the joint damping coefficient used in Simulation D. One cause of the simulations over-predicting jump height may be due to imperfect contact between the foot and jumping due to slippage during a jump. To eliminate this factor while parameterizing our jumping model, a third experiment was devised to eliminate its effect. In this experiment, the foot was fixed at a point and the leg was hung upside-down. The leg began in its extended state in this inverted configuration, and then pulled itself up by activating the motors to retract the leg. The resulting experimental data was used to determine the damping coefficient of the flexure joints. By iteratively comparing experimentally-collected trajectories across several leg designs against equivalent simulations, an optimal coefficient was determined that minimized trajectory error between simulated and experimental trajectories. The resulting matched trajectories are shown in Figure 5. By

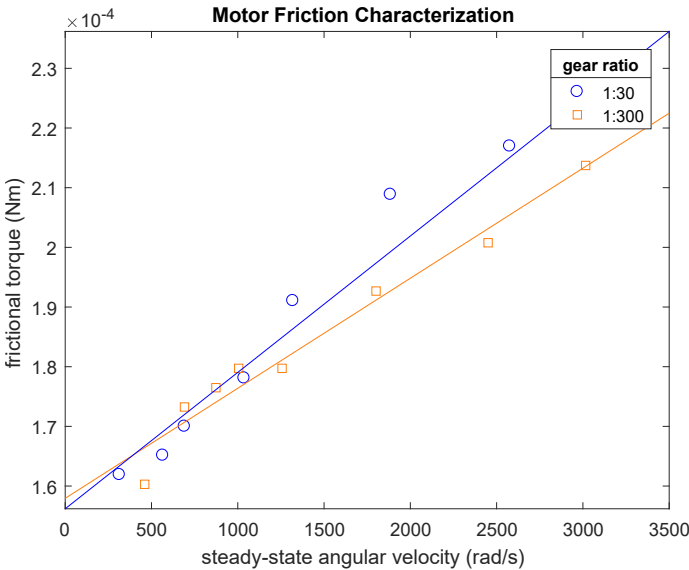


FIGURE 7: Friction characterization shows frictional torque for two different motor gearboxes at their full range of angular velocities. Both gearboxes have the same vertical offset suggesting a constant, non-viscous frictional force, and their linear relationship as the motor’s angular velocity increases indicates there is an additional linear damping component.

eliminating contact with the ground, a much closer fit was able to be achieved with the pull-ups than with jumping. The damping coefficient was then verified by comparing results from Experiment A to Simulation D, which included the optimal damping coefficient, as shown in Figure 8d. Including the damping in Simulation D resulted in the closest resemblance in trends between the simulated and experimental data.

4 Results and Discussion

The results from each of the four simulations were compared to the empirical results from Experiment A as shown in Figure 8. The dashed lines are the experimental results, and the solid lines are the simulation results. Simulations A and C, which modeled the leg with the same complexity but in different environments, both over-predict actual jump heights achieved by the prototype legs as seen in Figure 8a and 8c. However, the experimental and simulation trends show some resemblance. Comparing the theoretical and empirical results in both cases, lower gear ratios are optimized with shorter leg lengths. The scale of the predicted jump heights are vastly different than the experimental jump heights, however, suggesting that there is some inefficiency present in the physical design that is not present in Simulations A and C. Possible explanations include unmodeled dynamics of the motor and additional viscous damping in the leg joints. Each of these is explored respectively in Simulations B and D.

Simulation B incorporates a nonlinear motor model (described in detail in Section 2.3.2) as the possible source of this inefficiency in the physical leg. This significantly decreased the scale of the error and brought the predicted jump heights down into the range of the experimental jump heights. However, as seen in Figure 8b there is no resemblance between the trends in the experimental results and the predicted results from Simulation B.

The results of implementing the damping coefficient in Simulation D are shown in Figure 8d. A single coefficient was used for all leg lengths, assuming that the majority of the damping comes from joints rather than air drag, and is thus constant across identical joint geometries. Adding viscous joint damping resulted in significant improvement over Simulation C as shown by how the maxima within each design family more closely resemble the experimental maxima.¹

Since Simulation D presented the best combination of predicting both jump heights and design trends, Simulation D was then used to design a new, final leg. In Figure 9, Simulation D was run for all of the available motor gear ratios and all leg lengths suitable for these motors in order to find the globally optimal design for maximizing jump ground clearance. The range of design parameters was expanded further than the set of design parameters previously tested experimentally or in simulation.

The globally optimal design was found at a leg length between 12 cm and 14 cm paired with a 210:1 gear ratio. The predicted ground clearance at the peak of the jump was predicted to be 22 cm. A design with a 12 cm leg was selected because increasing the leg length offered little increase in jump ground clearance and negatively impacted the predicted jump height relative to leg length. When this leg was then constructed, it performed jumps with an average ground clearance of 18.3 cm over three tests.¹ The final leg design is shown in Figure 10.

The Pareto plot shown in Figure 11 was created using Simulation D. This tool allows the trade-off between ground clearance and relative height to be analyzed, following the logic that a shorter leg jumping is preferable to a longer leg jumping the same height. In this plot, optimal designs will appear along the Pareto front, while interior designs are sub-optimal. This plot was used to select the 12 cm leg over the 14 cm leg because in exchange for a small sacrifice in ground clearance, it offers a considerable improvement in relative height.

5 Conclusions and Future Work

This work has been conducted to determine whether a dynamics model can be used to determine performance trends for both interpolative and extrapolative designs and which model elements are necessary for achieving relatively good jump height estimates. Incorporating inertia and leg flexibility, as well as

¹The final design is shown in comparison with the simulation in this video

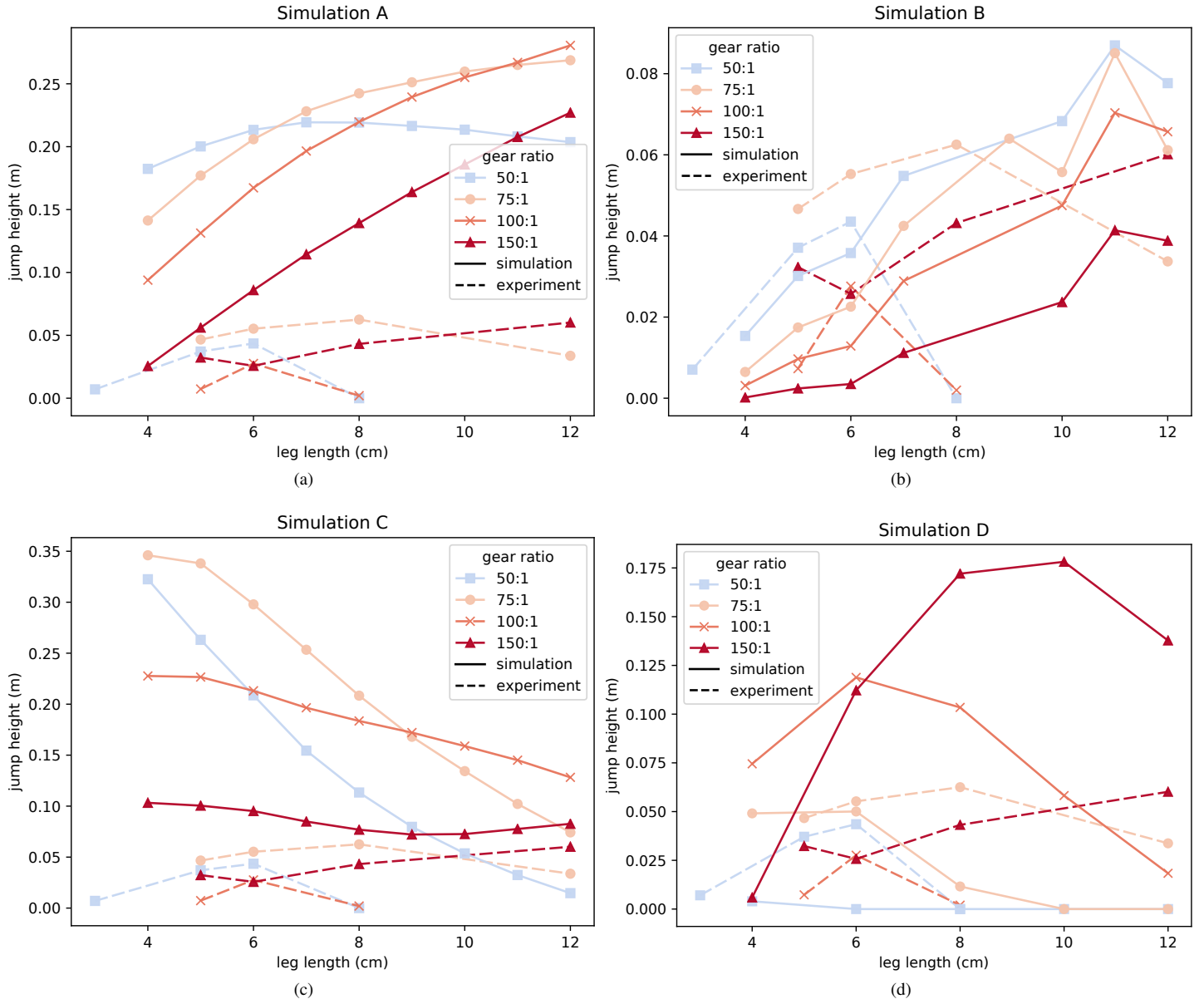


FIGURE 8: Simulations are compared with experimental results. (a) Simulation A. (b) Simulation B. (c) Simulation C. (d) Simulation D.

damping of leg joints improved the fidelity of the leg model considerably.

The model we ultimately selected is designed to be modular, relying on properties of leg materials and selected gear-motors, so that different materials or motors can be substituted by entering the appropriate constants. This same model can be used to select a design to meet different objectives, such as maximizing total height, or to search within a different design space than the motor or rigid material that was used for this design. Instead of

choosing the optimal design for ground clearance, another goal could be to achieve the greatest total height relative to the robot's leg length. An eight centimeter leg with a 150:1 motor gear ratio in that case would theoretically improve the relative jump height while sacrificing some ground clearance.

In future work, this model can be used to design the leg for other bipedal laminate robot tasks. In addition to predicting the performance of different motor-leg design combinations, the simulation will be used to evaluate proposed control systems for

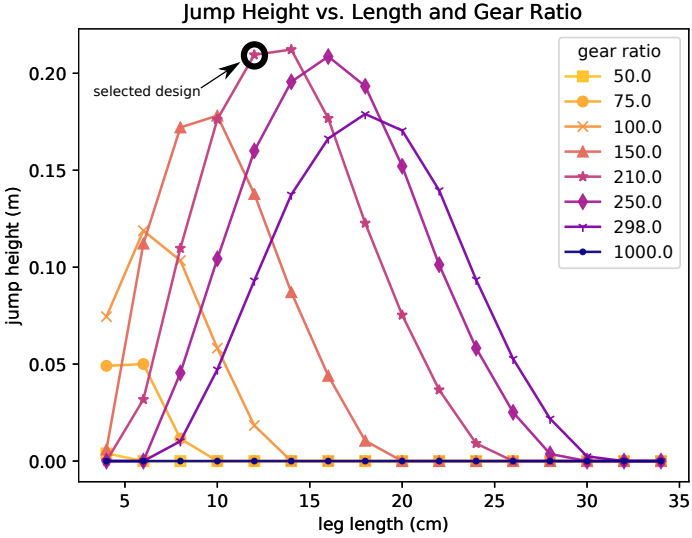


FIGURE 9: Search for globally optimal leg design across all available motor gear ratios and corresponding appropriate leg lengths. Results indicate a 210:1 gear ratio with a leg length between 12–14 cm achieves the global maximum jump ground clearance of 22 cm. The circled 12 cm leg design was chosen for the optimal prototype because increasing leg length offered a relatively small increase in jump height.

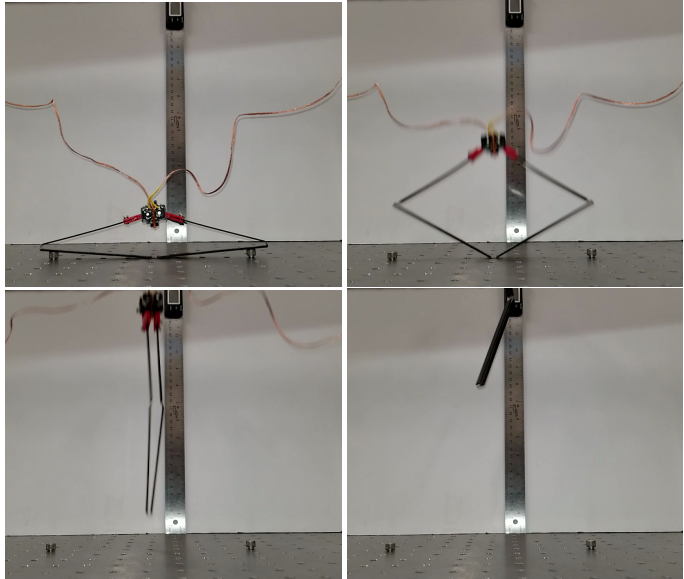


FIGURE 10: Optimal leg design as predicted by simulation performing a vertical jump from rest. The leg achieved a maximum ground clearance of 19 cm in this test and an average of 18.3 cm over three trials.

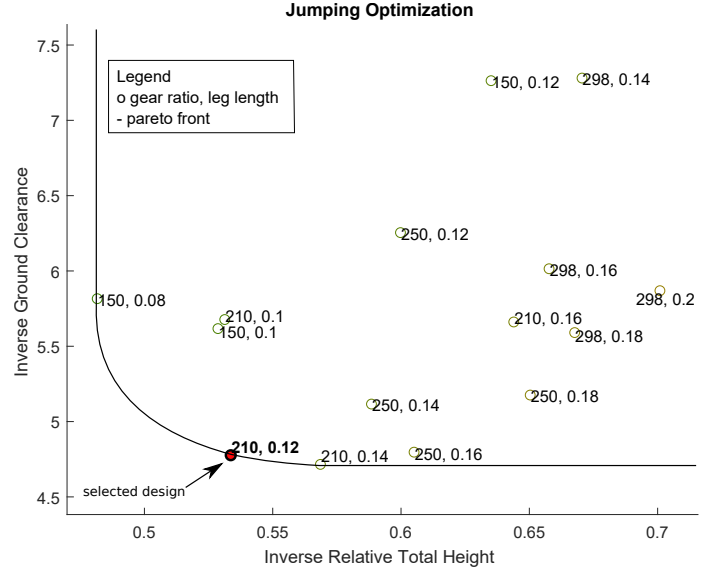


FIGURE 11: Pareto plot comparing jumping goals shows the trade-off between ground clearance and relative jump height. Only a few optimal designs appear along the Pareto front. The middle of these is highlighted because it was chosen as the final leg prototype.

actions like jumping and walking on two legs. While the current model uses the motors’ rated voltage as a control signal, future efforts would tie in control signals based on state-based feedback from the robot. In this way, different control signals can be simulated across each motor so that, rather than merely commanding the leg to jump, different walking patterns can be simulated in order to assess their speed and stability.

REFERENCES

- [1] Onal, C. D., Tolley, M. T., Wood, R. J., and Rus, D., 2015. “Origami-Inspired Printed Robots”. *IEEE/ASME Transactions on Mechatronics*, **20**(5), Oct., pp. 2214–2221.
- [2] Agheli, M., Faal, S. G., Chen, F., Gong, H., and Onal, C. D., 2014. “Design and fabrication of a foldable hexapod robot towards experimental swarm applications”. IEEE, pp. 2971–2976.
- [3] Birkmeyer, P., Peterson, K., and Fearing, R. S., 2009. “DASH: A dynamic 16g hexapodal robot”. In 2009 IEEE/RSJ International Conference on Intelligent Robots and Systems, pp. 2683–2689.
- [4] Zhang, J., Song, G., Li, Y., Qiao, G., Song, A., and Wang, A., 2013. “A bio-inspired jumping robot: Modeling, simulation, design, and experimental results”. *Mechatronics*, **23**(8), Dec., pp. 1123–1140.
- [5] Zhao, J., Xu, J., Gao, B., Xi, N., Cintrón, F. J., Mutka, M. W., and Xiao, L., 2013. “MSU Jumper:

- A Single-Motor-Actuated Miniature Steerable Jumping Robot". *IEEE Transactions on Robotics*, **29**(3), June, pp. 602–614.
- [6] Haldane, D. W., Plecnik, M., Yim, J. K., and Fearing, R. S., 2016. "A power modulating leg mechanism for monopodal hopping". In 2016 IEEE/RSJ International Conference on Intelligent Robots and Systems (IROS), pp. 4757–4764.
- [7] Scarfogliero, U., Stefanini, C., and Dario, P., 2009. "The use of compliant joints and elastic energy storage in bio-inspired legged robots". *Mechanism and Machine Theory*, **44**(3), mar, pp. 580–590.
- [8] Scarfogliero, U., Stefanini, C., and Dario, P., 2007. "Design and Development of the Long-Jumping "Grillo" Mini Robot". In Proceedings 2007 IEEE International Conference on Robotics and Automation, no. April, IEEE, pp. 467–472.
- [9] Kovač, M., Fuchs, M., Guignard, A., Zufferey, J. C., and Floreano, D., 2008. "A miniature 7g jumping robot". *Proceedings - IEEE International Conference on Robotics and Automation(c)*, pp. 373–378.
- [10] Koh, J. S., Jung, S. P., Noh, M., Kim, S. W., and Cho, K. J., 2013. "Flea inspired catapult mechanism with active energy storage and release for small scale jumping robot". *Proceedings - IEEE International Conference on Robotics and Automation*, pp. 26–31.
- [11] Niiyama, R., Nagakubo, A., and Kuniyoshi, Y., 2007. "Mowgli: A Bipedal Jumping and Landing Robot with an Artificial Musculoskeletal System". In Proceedings 2007 IEEE International Conference on Robotics and Automation, pp. 2546–2551.
- [12] Hubicki, C., Grimes, J., Jones, M., Renjewski, D., Spröwitz, A., Abate, A., and Hurst, J., 2016. "ATRIAS: Design and validation of a tether-free 3d-capable spring-mass bipedal robot". *The International Journal of Robotics Research*, **35**(12), Oct., pp. 1497–1521.
- [13] Okada, M., and Takeda, Y., 2012. "Optimal design of non-linear profile of gear ratio using non-circular gear for jumping robot". *Proceedings - IEEE International Conference on Robotics and Automation*, pp. 1958–1963.
- [14] Plecnik, M. M., Haldane, D. W., Yim, J. K., and Fearing, R. S., 2016. "Design Exploration and Kinematic Tuning of a Power Modulating Jumping Monopod". *Journal of Mechanisms and Robotics*, **9**(1), p. 011009.
- [15] Kenneally, G., De, A., and Koditschek, D. E., 2016. "Design Principles for a Family of Direct-Drive Legged Robots". *IEEE Robotics and Automation Letters*, **1**(2), jul, pp. 900–907.